Human Molecular Genetics, 2012 **1–14**
doi:10.1093/hmg/dds407

L-arginine:glycine amidinotransferase deficiency protects from metabolic syndrome

Chi-un Choe[1,2,†], Christine Nabuurs[3,†,‡], Malte C. Stockebrand[1], Axel Neu[1], Patricia Nunes[3], Fabio Morellini[1], Kathrin Sauter[1], Stefan Schillemeit[1], Irm Hermans-Borgmeyer[4], Bart Marescau[5], Arend Heerschap[3] and Dirk Isbrandt[1,*]

[1]Experimental Neuropediatrics, Center for Molecular Neurobiology and Department of Pediatrics and [2]Department of Neurology, University Medical Center Hamburg-Eppendorf, 20246 Hamburg, Germany, [3]Department of Radiology, Radboud University Nijmegen Medical Center, Nijmegen, The Netherlands, [4]Transgenic Animal Facility, Center for Molecular Neurobiology Hamburg, University Medical Center Hamburg-Eppendorf, 20246 Hamburg, Germany and [5]Laboratory of Neurochemistry and Behaviour, Born-Bunge Foundation, University of Antwerp, Antwerp, Belgium

Received May 18, 2012; Revised and Accepted September 24, 2012

Phosphorylated creatine (Cr) serves as an energy buffer for ATP replenishment in organs with highly fluctuating energy demand. The central role of Cr in the brain and muscle is emphasized by severe neurometabolic disorders caused by Cr deficiency. Common symptoms of inborn errors of creatine synthesis or distribution include mental retardation and muscular weakness. Human mutations in L-arginine:glycine amidinotransferase (AGAT), the first enzyme of Cr synthesis, lead to severely reduced Cr and guanidinoacetate (GuA) levels. Here, we report the generation and metabolic characterization of AGAT-deficient mice that are devoid of Cr and its precursor GuA. AGAT-deficient mice exhibited decreased fat deposition, attenuated gluconeogenesis, reduced cholesterol levels and enhanced glucose tolerance. Furthermore, Cr deficiency completely protected from the development of metabolic syndrome caused by diet-induced obesity. Biochemical analyses revealed the chronic Cr-dependent activation of AMP-activated protein kinase (AMPK), which stimulates catabolic pathways in metabolically relevant tissues such as the brain, skeletal muscle, adipose tissue and liver, suggesting a mechanism underlying the metabolic phenotype. In summary, our results show marked metabolic effects of Cr deficiency via the chronic activation of AMPK in a first animal model of AGAT deficiency. In addition to insights into metabolic changes in Cr deficiency syndromes, our genetic model reveals a novel mechanism as a potential treatment option for obesity and type 2 diabetes mellitus.

INTRODUCTION

The phosphocreatine (PCr)/creatine (Cr) system functions as a rapidly available buffer for ATP replenishment in organs of high and fluctuating energy demand. PCr and Cr [(P)Cr] are most abundant in the skeletal muscle at concentrations of 20–40 mM (1). Continuous non-enzymatic degradation of Cr to creatinine (Crn) at a daily rate of 1–2% necessitates exogenous dietary Cr intake or endogenous Cr synthesis. Cr biosynthesis is a two-step process occurring mainly in the kidney, pancreas and liver (1). In a first step, L-arginine:glycine amidinotransferase (AGAT, EC 2.1.4.1) synthetizes guanidinoacetate (GuA) from arginine and glycine. In a second step, GuA *N*-methyltransferase (GAMT, EC 2.1.1.2) methylates GuA to form Cr. Finally, Cr is distributed and actively taken up by different tissues via the Cr transporter (*SLC6A8*). Mutations in *AGAT* (OMIM 602360), *GAMT* (OMIM 601240) or *SLC6A8* (OMIM 300352) underlie hereditary Cr deficiency syndromes characterized by mental retardation and muscle weakness (2–4).

*To whom correspondence should be addressed at: Experimental Neuropediatrics, Center for Molecular Neurobiology and Department of Pediatrics, University Medical Center Hamburg-Eppendorf, Martinistr. 52, 20246 Hamburg, Germany. Tel: +49-40-741056650; Fax: +49-40-741056263; Email: dirk.isbrandt@enp.org
†The authors wish it to be known that, in their opinion, the first two authors should be regarded as joint First Authors.
‡Current affiliation: NUTRIM School of Nutrition, Toxicology and Metabolism, Maastricht University Medical Center, Maastricht.

A number of mouse models with single and double Cr kinase (CK) subunit deficiencies have elucidated the role of the Cr/CK system in the skeletal muscle, brain and heart. However, due to the existence of four CK isoforms, the complete and systemic (P)Cr depletion has not yet been achieved (5–8). We previously generated a mouse model of GAMT deficiency showing complete and systemic lack of Cr (9). However, GAMT-deficient mice accumulated significant amounts of phosphorylated GuA, which could partially substitute for (P)Cr (10). Thus, we decided to block the first step of Cr synthesis by generating AGAT-deficient mice to avoid the accumulation of any energy-buffering guanidino compounds.

CK-deficient and GAMT-deficient mice are smaller and lighter in weight than their littermates, indicating an altered energy metabolism. As intracellular high-energy phosphates such as ATP and (P)Cr are known to control signaling cascades regulating cellular and whole-body energy metabolism (11,12), we hypothesized that the depletion of (P)Cr stores could alter glucose and lipid metabolism, the dysfunction of which underlies type 2 diabetes mellitus (T2DM) and obesity.

Therefore, we generated and analyzed AGAT-deficient mice focusing on their metabolic phenotype and taking advantage of the temporary and reversible replenishment of the Cr pool by oral Cr supplementation. In our AGAT-deficient mouse model, we show that Cr deficiency results in attenuated gluconeogenesis, reduced cholesterol levels, enhanced glucose tolerance and complete protection from diet-induced obesity (DIO). Our data suggest that metabolic effects of Cr deficiency syndromes are mediated via the chronic activation of AMP-activated protein kinase (AMPK) in tissues such as skeletal muscle and adipose tissue. In addition, this mechanism might prove valuable for the treatment of metabolic syndrome, including T2DM and obesity.

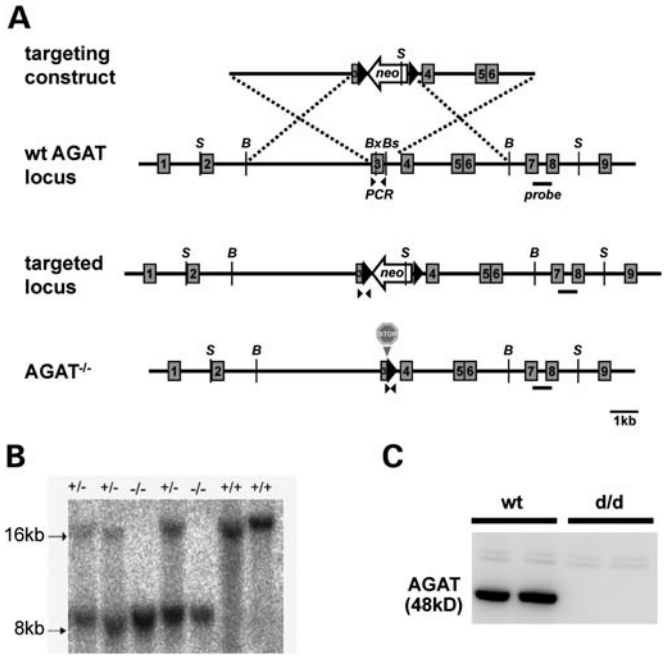

Figure 1. Generation of AGAT mice. (**A**) To disrupt the murine AGAT locus by gene targeting, exon 3 was replaced with a selection cassette containing the neomycin resistance gene (Neo) flanked by Lox-P sites, as described in Materials and methods. (**B**) Southern blot analysis of the AGAT gene in heterozygous and homozygous AGAT knockout mice reveals predicted restriction fragments. (**C**) Western blot analysis reveals the absence of the AGAT protein in kidney lysates of d/d mice.

RESULTS

Generation of AGAT mice with reversible Cr depletion

To achieve complete (P)Cr and (P)GuA depletion in mice, we genetically disrupted *AGAT*, the first enzyme of Cr biosynthesis. Disruption of the murine *AGAT* gene was confirmed by Southern blot analysis and the absence of the AGAT protein in western blot (Fig. 1). AGAT$^{-/-}$(d/d) mice were viable and did not require any specific treatment for survival or growth. Breeding did not lead to offspring from d/d females or males. Histological sections from testis revealed impaired spermatogenesis and comparable structural abnormalities as previously seen in GAMT knockout mice (Supplementary Material, Fig. S1). Heterozygous breeding revealed AGAT genotype frequencies characterized by a Mendelian inheritance pattern [wild-type (wt), 24.9%; heterozygous, 51.0%; d/d, 24.1%; $n = 1388$]. *In vivo* skeletal muscle ^{1}H magnetic resonance (MR) spectroscopy of d/d mice confirmed (P)Cr depletion ([total Cr]: wt 28.9 ± 2.9 mM, d/d 4.1 ± 1.5 mM, $P < 0.01$ (wt versus d/d), Fig. 2A and B). (P)Cr concentrations returned to wt levels in the skeletal muscle on oral Cr supplementation of d/d mice (d/d + Cr) ([total Cr]: 22.7 ± 2.0 mM; Fig. 2A and B bottom). Biochemical analysis of urine from d/d mice confirmed the systemic depletion of Cr, Crn and GuA (Fig. 2C). Although Cr and Crn levels did not differ between wt and d/d + Cr mice, GuA levels in d/d + Cr mice were still comparable with d/d mice (Fig. 2C). Together, MR spectroscopy and biochemical analysis confirm the systemic depletion of Cr and GuA in AGAT-deficient mice. In addition, Cr deficiency in d/d mice was reversed by oral Cr administration and is thus Cr-dependent.

Cr deficiency leads to a reduction in body weight and fat content

Systemic Cr deficiency resulted in a marked metabolic phenotype. The d/d mice were lean and short and had a markedly reduced body mass index (BMI; Fig. 2D–F). From 4 weeks of age onward, d/d mice showed consistently lower body weight (Fig. 3A and B). No weight difference was observed between wt and heterozygous mice (data not shown). The body composition analysis of d/d mice revealed reduced fat content (Fig. 3C), which was accompanied by lower serum levels of the adipose-derived anorexigenic hormone leptin and increased food intake (leptin: wt 12.2 ± 8.1 ng/ml, d/d 3.9 ± 2.7 ng/ml, $P < 0.001$; absolute food intake: wt 3.6 ± 0.2 g/24 h, d/d 4.3 ± 0.1 g/24 h, $P < 0.001$; Fig. 3D). The decreased body weight could not be explained by malabsorption (feces energy content: wt 16.5 ± 0.05 kJ/g, d/d 16.4 ± 0.04 kJ/g), glucosuria (urine analysis reagent strip: wt negative, d/d negative) or changes in other metabolic parameters such as body temperature (rectal temperature: wt 37.1 ± 0.2°C, d/d 37.0 ± 0.1°C, $P = 0.68$), free triiodothyronine (fT3: wt 1.45 ± 0.13 pg/ml, d/d 1.31 ± 0.16 pg/ml, $P =$

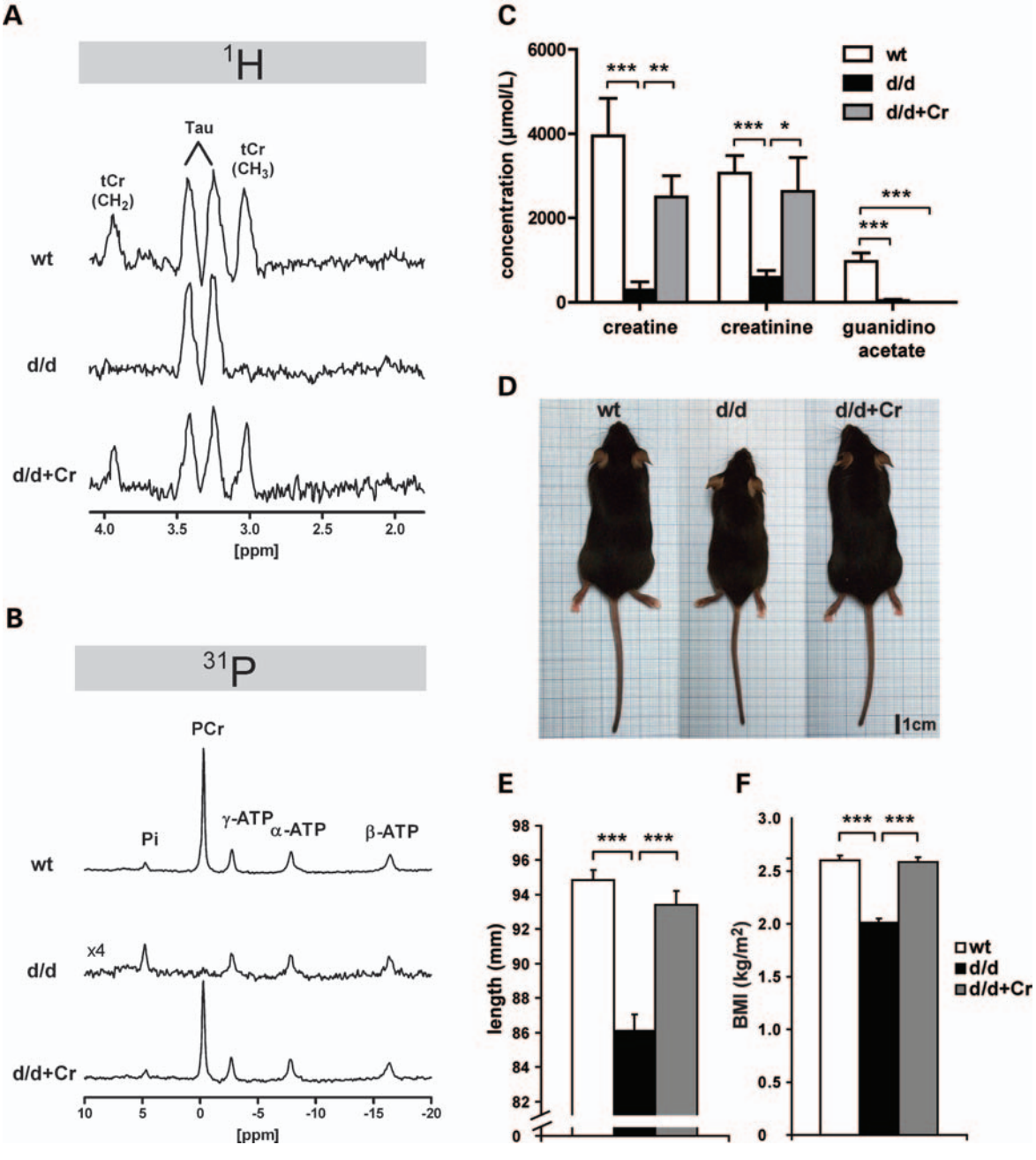

Figure 2. AGAT-deficient mice are Cr deficient. Representative ^{1}H (**A**) and ^{31}P (**B**) MR spectra of hind limb muscle in wt, d/d and Cr supplemented d/d (d/d + Cr) mice (×4 indicates four-fold *y*-axis magnification; tCr, total creatine; Tau, taurine; Pi, inorganic phosphate) ($n = 3$). (**C**) Concentrations of Cr, Crn and GuA in 24 h urine of wt, d/d and d/d + Cr mice. Representative pictures (**D**), snout-anus length (**E**) and BMI (**F**) of 20-week-old wt, d/d and d/d + Cr female littermates ($n = 16$–21). Data are expressed as mean ± SEM. Statistical significance between indicated conditions ($^{*}P < 0.05$; $^{**}P < 0.01$; $^{***}P < 0.001$).

0.54) or adiponectin serum levels (wt 125.3 ± 7.2 μg/ml, d/d 122.2 ± 4.7 μg/ml, $P = 0.71$). The locomotor activity of d/d mice was even reduced during the active dark period (dark phase: wt 40.8 ± 4.2%, d/d 29.3 ± 3.3%, $P < 0.05$; Fig. 3D). In addition, reduced body tension and severe scoliosis were observed, indicating chronic muscular hypotonia. Unlike d/d mice, d/d + Cr mice resembled wt mice with respect to body length, body weight, BMI and body composition (Fig. 2 and 3). Hence, the AGAT-deficient mouse model reported here is characterized by complete and reversible Cr deficiency associated with decreased body weight and fat content.

Cr deficiency protects from metabolic syndrome

The decreased body fat content in d/d mice prompted us to investigate whether adiposity could be induced by a high fat diet (HFD)—a widely used experimental model for DIO and metabolic syndrome. Therefore, we investigated whether d/d mice would become obese when put on a HFD. After 8 weeks of

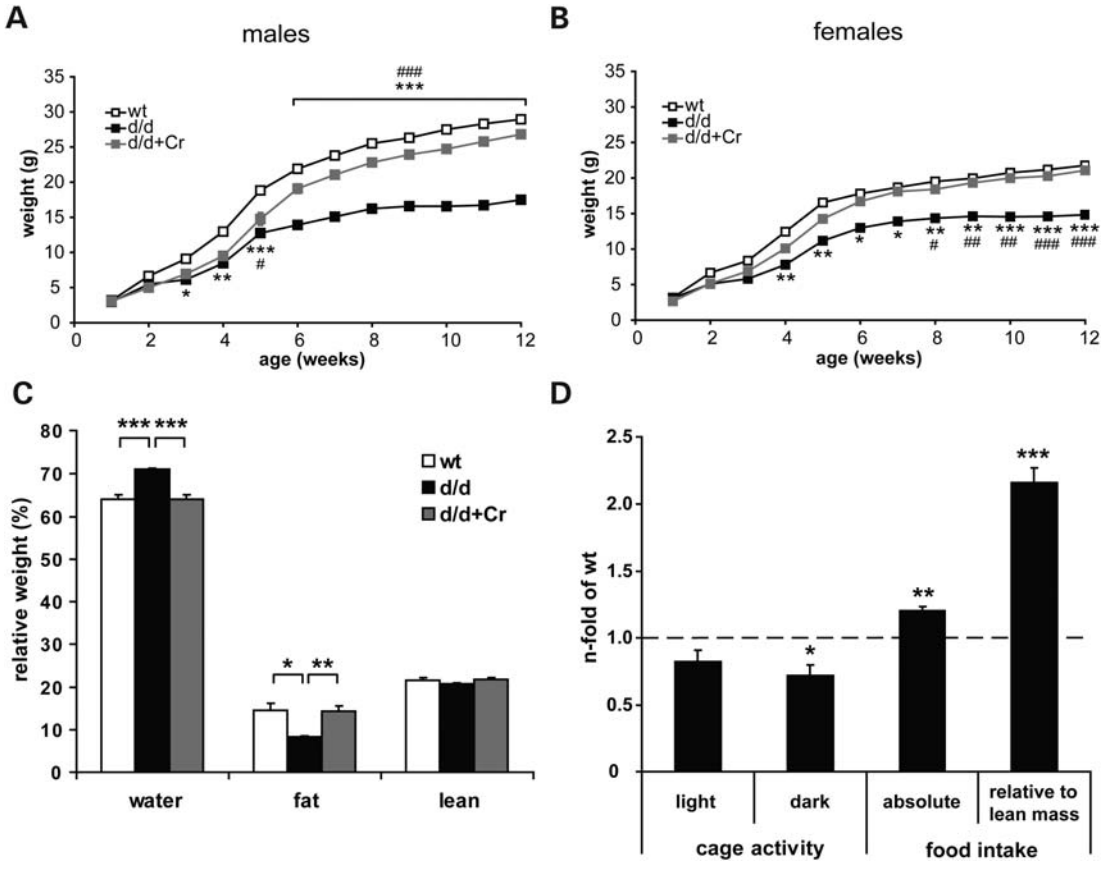

Figure 3. AGAT-deficient mice have reduced body weight and fat content. Body weight development of male (**A**) and female (**B**) animals until 12 weeks of age ($n = 7–26$). (**C**) Body composition analysis of water, fat and lean mass in wt, d/d and d/d + Cr mice ($n = 6–13$). (**D**) Comparison of cage activity, absolute and relative food intake of d/d mice normalized to wt levels indicated by dashed line ($n = 9–12$). Data are expressed as the mean ± SEM. Statistical significance between d/d versus wt (*), d/d versus d/d + Cr ($^{\#}$) or between indicated conditions ($^{*,\#}P < 0.05$; $^{**,\#\#}P < 0.01$; $^{***,\#\#\#}P < 0.001$).

HFD, the weight of wt mice (wt HFD) nearly doubled, whereas the weight of d/d mice (d/d HFD) did not change (Fig. 4A). In contrast, Cr supplementation of d/d mice on HFD (d/d + Cr HFD) resulted in a pronounced increase in body weight (Fig. 4B). Body composition analysis of d/d HFD mice revealed reduced fat content compared with wt and d/d + Cr mice on HFD, which can mainly be attributed to reduced epigonadal white adipose tissue (WAT) depots (Fig. 4C and D). As DIO is normally associated with increased lipid deposition in non-adipose tissues, we determined the liver fat content in wt and d/d on HFD. While wt mice on HFD exhibited hepatic steatosis, d/d mice on HFD showed only discrete lipid deposition in the liver (Fig. 4E). Hence, Cr deficiency protects from excessive lipid storage in both adipose and ectopic liver tissue.

Furthermore, the hepatic triglyceride (HTG) content and the contribution of hepatic *de novo* lipogenesis (DNL) to the total HTG content were determined by *in vitro* nuclear magnetic resonance spectroscopy (NMR) measurements. In line with histological findings, the HTG pool was significantly decreased in d/d compared with wt mice (Table 1). ^{2}H NMR measurements using $^{2}H_2O$ as a DNL tracer revealed higher ^{2}H enrichment of the HTG in d/d mice, which was not attributable to the increased lipid synthesis via DNL (14.9 ± 9.4 μmol/g wet weight (ww) for wt mice versus 17.1 ± 7.3 μmol/g ww for d/d mice) but to the reduced HTG pool of d/d mice. These data suggest higher hepatic β-oxidation or triglyceride output via very low-density lipoprotein. Based on the assumption that the remaining (unlabeled) HTG pool predominantly reflects a dietary lipid contribution during *ad libitum* feeding, only a minor fraction of dietary lipid is likely to end up as triglycerides in hepatic tissue of Cr-deficient mice. Hence, free fatty acids seem to be redirected to other energy-demanding tissues (e.g. skeletal muscle). The increase in circulating triglycerides on Cr supplementation of d/d mice is another indication of an altered lipid handling under the Cr-deficient condition (Fig. 4F). Since the liver is also the primary source of endogenous cholesterol synthesis, we measured cholesterol serum levels and found reduced concentrations in d/d mice under HFD conditions and normalized levels on Cr supplementation (Fig. 4G). Cr deficiency thus leads to reduced adipose and non-adipose lipid deposition and ultimately to protection from DIO.

Cr deficiency improves glucose tolerance

In addition to obesity and hyperlipidemia, impaired glucose tolerance and diabetes are hallmarks of the metabolic syndrome. We therefore investigated whether Cr deficiency is associated with abnormalities in glucose homeostasis in these mice. This was studied on both normal and HFD.

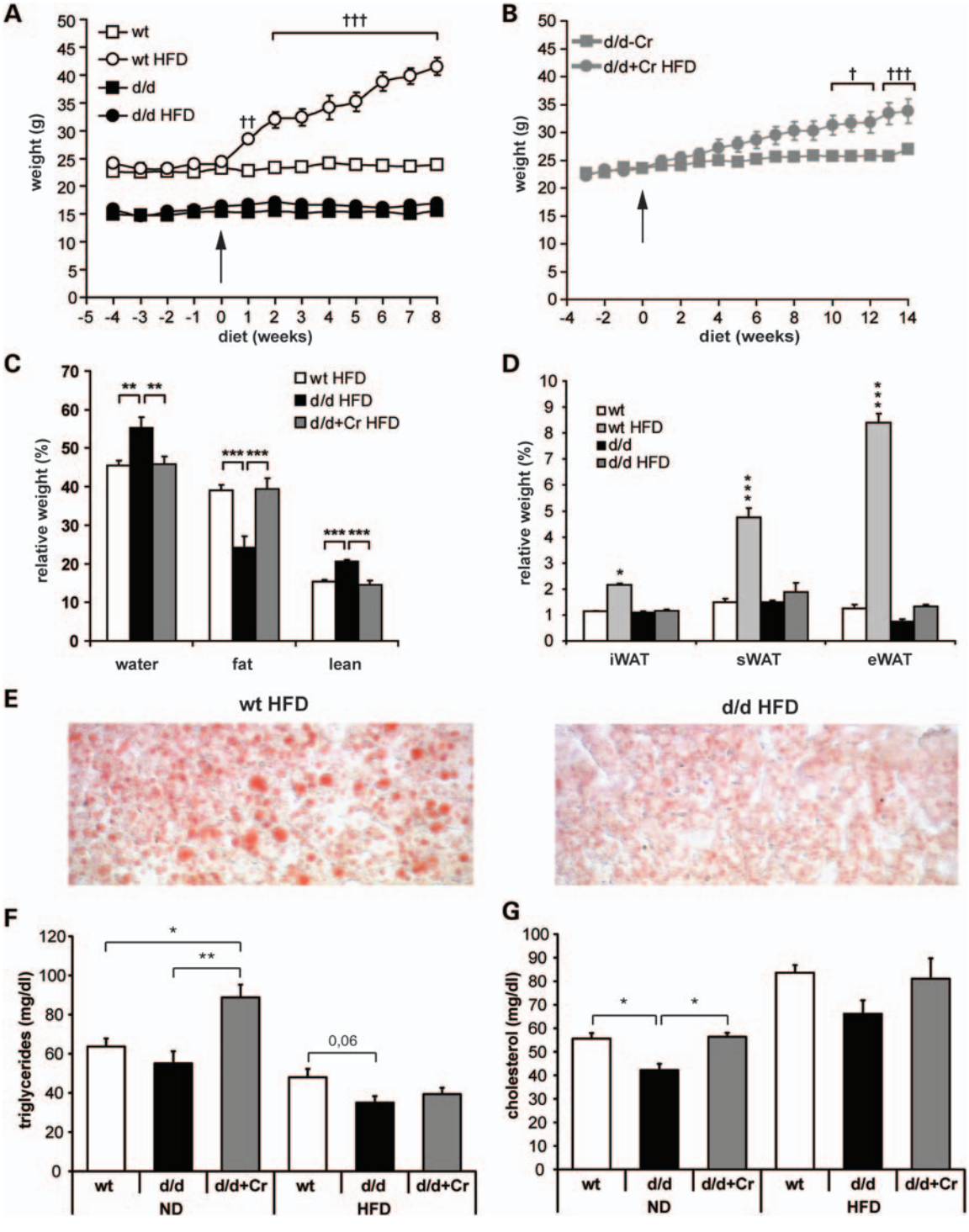

Figure 4. Cr-deficient mice are resistant to DIO. Weight development of wt, wt HFD, d/d and d/d HFD (**A**) as well as of d/d + Cr and d/d + Cr HFD mice (**B**) ($n = 6–14$). Arrows indicate start of HFD. Quantitative analysis of body composition (**C**) and different adipose tissues (iWAT, intestinal WAT; sWAT, subcutaneous WAT; eWAT, epigonadal WAT) (**D**) in animals on normal or HFD ($n = 6–7$). (**E**) Representative Sudan black liver staining of wt (left) and d/d mice (right) on HFD ($n = 3$). Cholesterol (**F**) and triglyceride (**G**) levels were determined in fasted wt, d/d and d/d + Cr under normal diet and HFD ($n = 5–15$). Data are expressed as the mean ± SEM. Statistical significance between d/d versus wt (*), normal versus HFD (†) or between indicated conditions (*,$^{\dagger}P < 0.05$; **,$^{\dagger\dagger}P < 0.01$; ***,$^{\dagger\dagger\dagger}P < 0.001$).

Glucose tolerance tests revealed faster glucose clearance in d/d mice on a normal diet (Fig. 5A). Whereas wt and, to a lesser degree, d/d + Cr animals developed glucose intolerance on HFD, d/d mice continuously showed accelerated glucose clearance (Fig. 5B). Increased insulin sensitivity in d/d mice was excluded by unaltered insulin tolerance tests (Fig. 5C).

Table 1. HTG content and DNL fractional synthesis

	Wt	AGAT$^{-/-}$
[HTG] (μmol/g ww)	195 ± 20	106 ± 19*
^{2}H body water fractional enrichment (%)	2.51 ± 0.15	2.38 ± 0.30
^{2}H HTG fractional enrichment (%)	0.19 ± 0.05	0.36 ± 0.15*
DNL synthesis (μmol/g ww)	14.9 ± 9.4	17.1 ± 7.3
Non-DNL (μmol/g ww)	180.0 ± 43.0	89.1 ± 44.3**

Values in mean ± SD. WT $n = 6$, AGAT $n = 5$, all males. Data were determined from ^{1}H and ^{2}H NMR spectra using 1.1% ^{2}H-enriched pyrazine as an internal reference. Significance levels when compared with wt mice on a ND.
*$P < 0.05$, *t*-test.
**$P < 0.01$, *t*-test.

Insulin levels in d/d mice, too, were comparable with wt mice under fasted conditions, but were even lower in d/d mice compared with wt and d/d + Cr mice after glucose challenge or when fed *ad libitum* (Fig. 5D). Given the attenuated blood glucose increase, we next investigated the steady-state GLUT4 protein levels. Quantitative western blot analysis revealed elevated GLUT4 levels in skeletal muscle and WAT of d/d mice (Fig. 5E and F). In addition to increased glucose clearance through GLUT4, gluconeogenesis in the liver significantly contributes to glucose homeostasis. Pyruvate tolerance tests (PTTs), indeed, showed impaired gluconeogenesis in d/d mice, which was normal in d/d + Cr mice (Fig. 5G). In addition to insulin, we analyzed serum levels of glucagon—the most important glucose-increasing hormone (13). Glucagon levels under fasted conditions and 30 min after glucose injection did not differ between wt, d/d and d/d + Cr mice (Fig. 5H). In conclusion, enhanced glucose tolerance in d/d mice does not result from increased insulin sensitivity, decreased glucagon levels or elevated insulin secretion, but is rather a consequence of increased glucose uptake via GLUT4 and impaired gluconeogenesis.

Cr deficiency results in chronic AMPK activation

Body energy homeostasis depends on complex processes regulating caloric intake and expenditure. A key sensor and regulator of energy metabolism is AMPK. AMPK activation by phosphorylation is promoted by increased intracellular AMP:ATP and Cr:PCr ratios, which reflect elevated cellular energy demand (11,14). We hypothesized that the depletion of (P)Cr stores would stimulate AMPK activity possibly via an increase in the intracellular AMP:ATP ratio.

In addition to complete Cr depletion (Fig. 2), AGAT-deficient mice had reduced muscular nucleoside triphosphate (NTP) concentrations compared with wt mice (NTP/volume in d/d was 63 ± 8% of wt, $P < 0.001$). In agreement with our hypothesis, phosphorylated and thus activated AMPK (pAMPK) levels were increased in the skeletal muscle, WAT and liver of d/d mice (Fig. 6A–F). Cr supplementation normalized the (P)Cr pool (Fig. 1 bottom) and, most importantly, returned AMPK activation in d/d + Cr to wt levels (Fig. 6A–F). Furthermore, acetyl-CoA-carboxylase (ACC), a prominent downstream target of AMPK (15), was inhibited by increased phosphorylation in the skeletal muscle, WAT and liver of Cr-deficient but not Cr-supplemented d/d mice (Fig. 6A–F). Consistent with increased basal AMPK phosphorylation, the 5-amino-1-β-D-ribofuranosyl-imidazole-4-carboxamide (AICAR)-induced decrease in blood glucose levels was less pronounced in d/d mice (Fig. 6G). Thus, the genetic disruption of Cr synthesis led to reversible, chronic and systemic AMPK activation, correlating with the metabolic phenotype in d/d mice.

Brain Cr deficiency results in chronic AMPK activation in the hypothalamus

Recent results have revealed a pivotal role of the hypothalamus for whole-body metabolism (16). Therefore, we also investigated whether AGAT deficiency also results in chronic hypothalamic AMPK activation. The *in vivo* brain ^{1}H MR spectroscopy of d/d mice revealed Cr deficiency in selected subcortical brain areas ([total Cr]: wt 11.4 ± 1.5 mM, d/d 1.5 ± 1.2 mM, $P < 0.01$ (wt versus d/d), Fig. 7A–C). Total brain Cr concentrations, similar to those in the skeletal muscle, returned to wt levels in d/d + Cr ([total Cr]: 11.9 ± 2.0 mM; Fig. 7A–C). Likewise, as in the skeletal muscle, liver and WAT, the depletion of the Cr pool in the brain resulted in increased phosphorylated and thus activated AMPK levels (Fig. 7D and E). Cr supplementation significantly reduced pAMPK levels to wt levels in d/d + Cr mice. Thus, AGAT deficiency resulted in both brain Cr deficiency and reversible and chronic hypothalamic AMPK activation.

DISCUSSION

The consequences of Cr deficiency syndromes and, in particular, the impact of the (P)Cr pool in regulating the whole-body energy homeostasis are incompletely understood. Although Cr deficiency is generally believed to be detrimental to cell and organ function, our present study surprisingly reveals that systemic Cr deficiency in mice leads to enhanced glucose tolerance and complete protection from DIO. All metabolic parameters were reversible upon Cr supplementation. Our data strongly suggest that these effects are mediated by chronic AMPK activation in metabolically important organs such as the brain, skeletal muscle, WAT and liver.

Mouse models for Cr deficiency

Here, we report on the generation of AGAT-deficient mice and show that AGAT deficiency in mice results in the systemic depletion of Cr, which is reversible on dietary Cr supplementation. Heterozygous breeding followed a Mendelian inheritance pattern, while d/d mice were infertile. As in GAMT$^{-/-}$, infertility can be attributed to impaired spermatogenesis in AGAT$^{-/-}$ mice (9). In contrast, the proportion of GAMT-deficient offspring from heterozygous breeding was 14.5% and thus strongly deviated from the Mendelian ratio (9). This difference in perinatal survival might be caused by the accumulation of GuA reaching neurotoxic levels in GAMT-deficient mice, which has been shown to interfere with GABAergic neurotransmission (17). The d/d mice, in

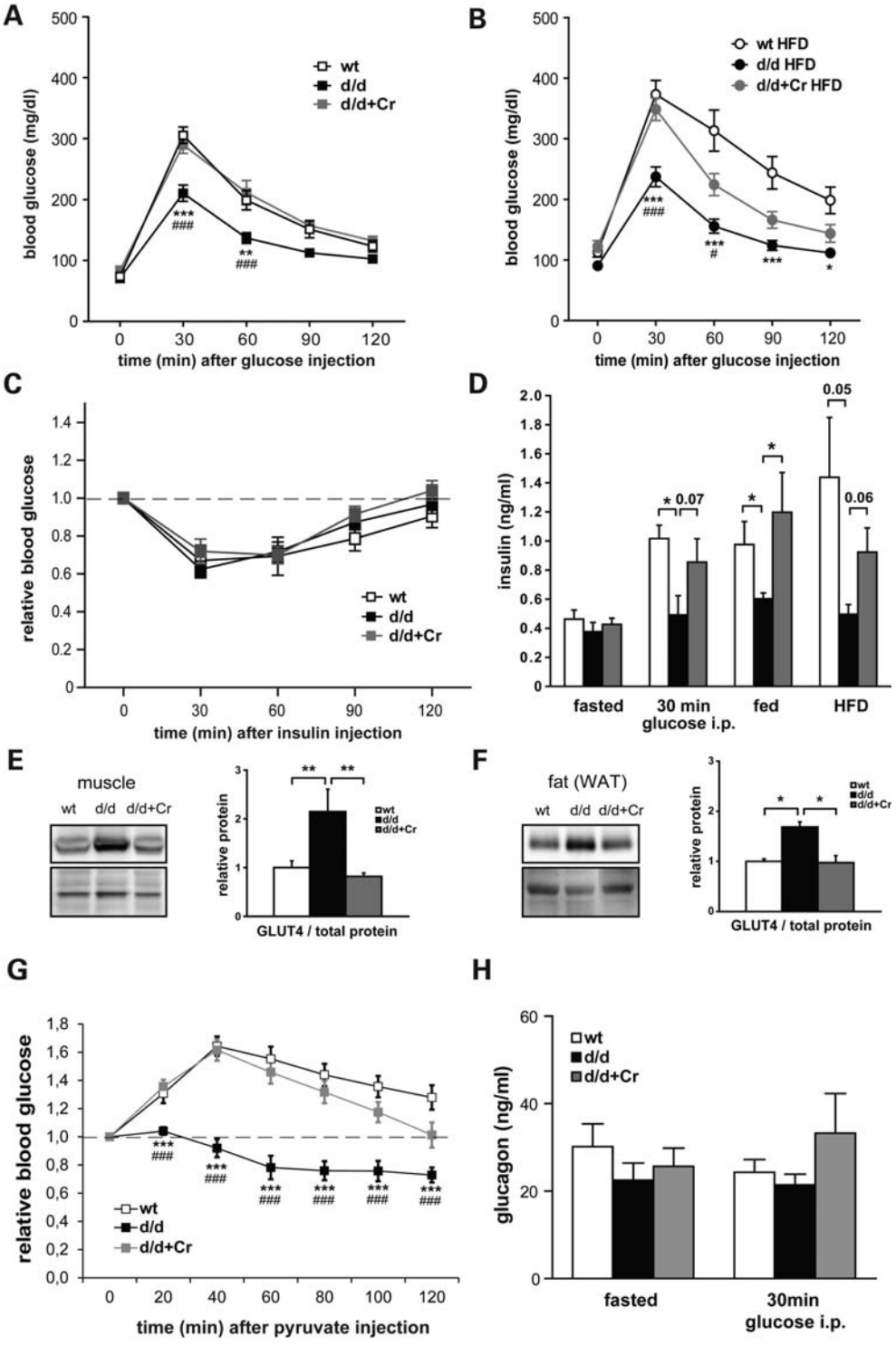

Figure 5. Cr deficiency improves glucose tolerance. Glucose tolerance test in wt, d/d and d/d + Cr mice on normal diet (**A**) and HFD (**B**) ($n = 10–13$). (**C**) Insulin tolerance test (0.25 IU/g body weight) in fasted wt, d/d and d/d + Cr mice ($n = 10–13$). (**D**) Insulin secretion of fasted, glucose-injected, *ad libitum*-fed on ND-fed as well as fasted on HFD-fed wt, d/d and d/d + Cr animals ($n = 7–9$). Representative western blots (left) and quantitative analysis (right) of GLUT4 normalized to protein content from skeletal muscle (**E**) and WAT (**F**) ($n = 3–8$). (**G**) Pyruvate tolerance (2 mg/g body weight) test in fasted wt, d/d and d/d + Cr mice ($n = 10–13$). (**H**) Glucagon levels of fasted and glucose-injected wt, d/d and d/d + Cr animals ($n = 6$). Data are expressed as the mean ± SEM. Statistical significance between normal versus HFD (*), d/d versus d/d + Cr (#) or between indicated conditions: $^{*,\#}P < 0.05$; $^{**}P < 0.01$; $^{***,\#\#\#}P < 0.001$ ($n = 9–13$).

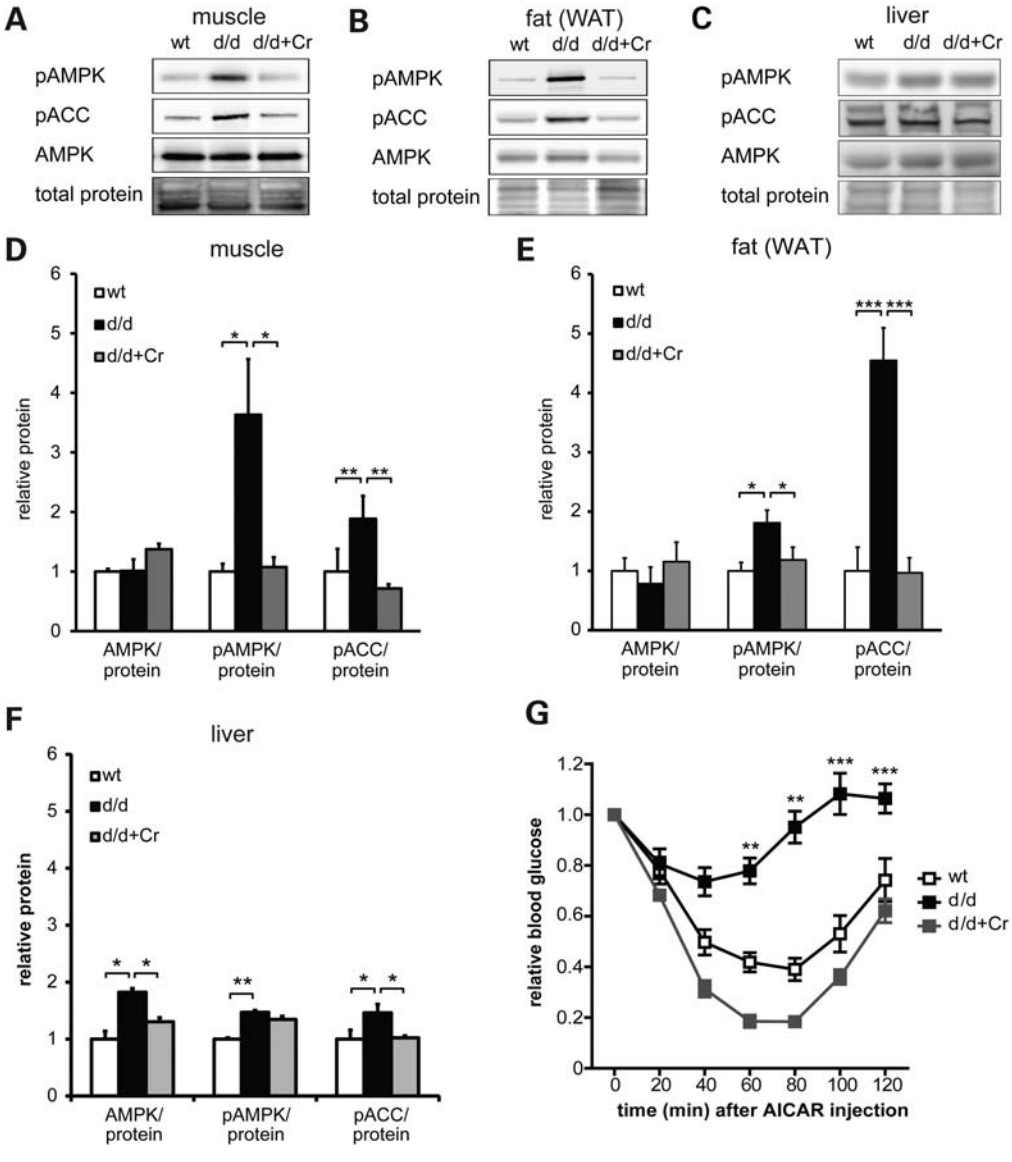

Figure 6. Cr-deficient mice show chronic AMPK activation. Representative western blots of pACC, pAMPK, AMPK and total protein from the skeletal muscle (**A**), fat (WAT) (**B**) and liver (**C**) ($n = 3–8$). Quantification of AMPK, pAMPK and pACC from the skeletal muscle (**D**), WAT (**E**) and liver (**F**) normalized to total protein ($n = 3–8$). (**G**) AICAR tolerance test in wt, d/d and d/d + Cr mice ($n = 5–10$). Data are expressed as the mean ± SEM. Statistical significance between wt and d/d or between indicated conditions ($^{*}P < 0.05$, $^{**}P < 0.01$, $^{***}P < 0.001$).

contrast, were devoid of GuA (Fig. 2C) (9). In addition, the normal body weight development of d/d mice until 3 weeks of age is indicative of normal development during the early postnatal period (Fig. 3), which may be ascribed to prenatal and early post-natal Cr supplementation by heterozygous mothers.

Although our targeting strategy yielded a constitutive AGAT knockout, a major advantage of this model is the complete reversibility of Cr deficiency, as shown by MR spectroscopy and biochemical analysis (Fig. 2). Oral Cr supplementation resulted in complete normalization of body weight and body composition in d/d mice (Fig. 3). Furthermore, enhanced glucose tolerance of d/d mice returned to wt levels on oral Cr supplementation (Fig. 5). Above all, Cr replenishment rendered d/d mice partially susceptible to DIO (Fig. 4). Our data show that the replenishment of the Cr pool via oral Cr supplementation led to normalization of metabolic alterations in d/d mice. Therefore, our AGAT-deficient mouse model displays aspects of conditional mouse models functioning as a 'Cr ON/OFF' system. Hence, the effects of Cr depletion in this mouse model are not caused by adaptations during development.

Mouse models for chronic AMPK activation

Body energy homeostasis depends on a careful regulation of caloric intake and expenditure. A key sensor and regulator of energy metabolism is AMPK. Energy-demanding processes such as hypoxia, muscle contraction and ischemia activate AMPK-promoting catabolic and AMPK-inhibiting anabolic

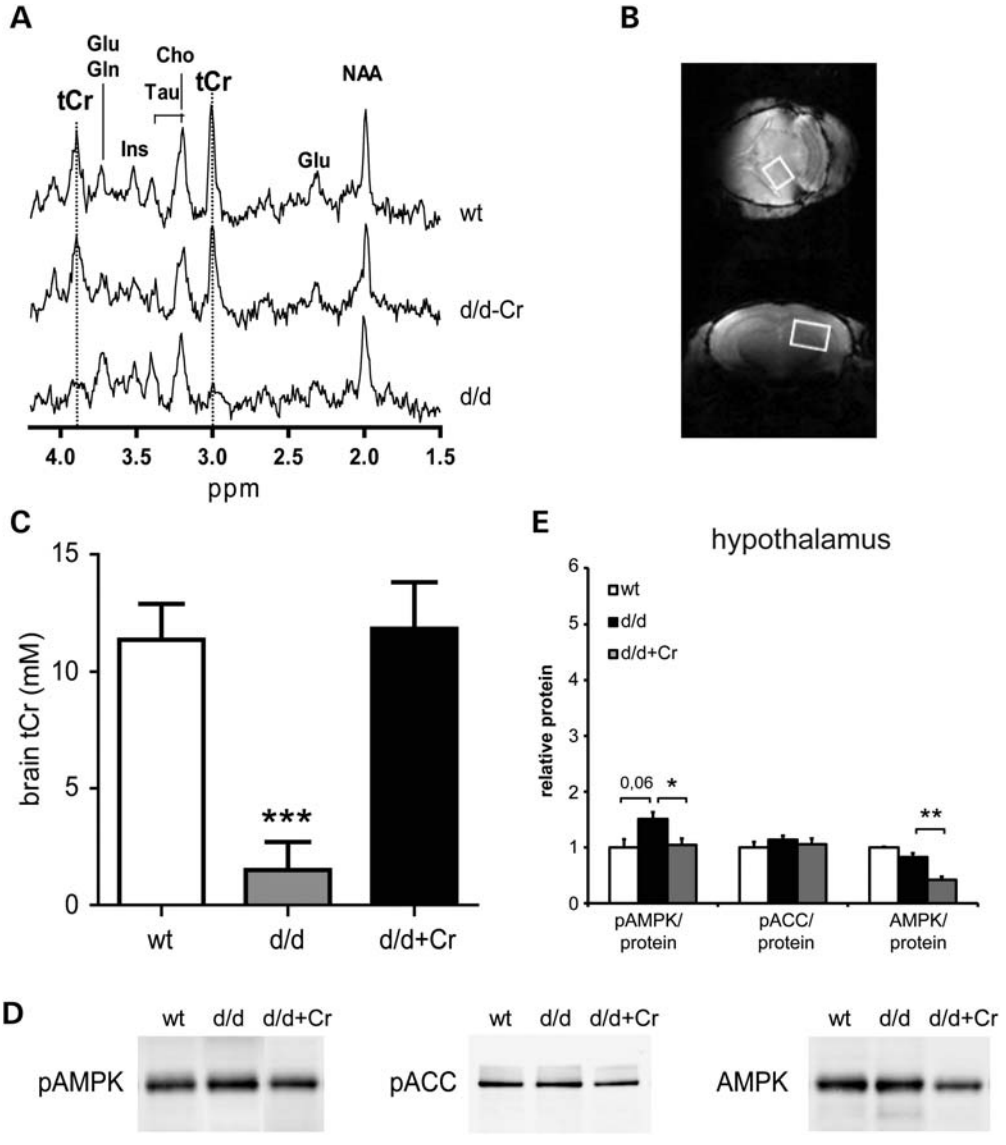

Figure 7. Brain Cr deficiency results in hypothalamic AMPK activation. (**A**) The lower two STEAM-localized ^{1}H MR spectra were obtained from the thalamus/hippocampus region of the same knockout mouse before (lower) and after 21 days of Cr supplementation (middle) [voxel size = 8.8 μl, repetition time (TR) = 5 s, 256 average, 5 Hz Lorentzian apodization, 7 T MR systems]. (**B**) The STEAM-localized spectra (voxel size = 8.8 μl, TR = 5 s, 256 average, 5 Hz Lorentzian apodization, 7 T MR systems) were acquired in the thalamus/hippocampus region as shown in gradient echo MR images in transversal [repetition time/echo time (TR/TE) = 4000/10 ms, four slices of 1 mm, FOV 15 × 15 mm, 128 × 128 matrix) and coronal (TR/TE = 4000/4 ms, 1 mm slices, FOV 12 × 12 mm, 64 × 64 matrix] directions. (**C**) Bar graph of cerebral total Cr (tCr) levels in wt, d/d and d/d + Cr for 21 days ($n = 5$ per group). Note the absence of tCr in d/d mice is rescued after 21 days of Cr supplementation ($^{***}P < 0.001$ compared with wt and d/d + Cr). (**D**) Representative western blots of pAMPK, pACC and AMPK from the hypothalamus ($n = 3–5$). (**E**) Quantification of pAMPK, pACC and AMPK normalized to total protein ($n = 3–5$) ($^{*}P < 0.05$, $^{**}P < 0.01$).

processes. In glucose metabolism, AMPK increases glucose uptake into skeletal muscle via GLUT4 and inhibits gluconeogenesis, eventually reducing blood glucose levels (12). In lipid metabolism, AMPK increases lipid oxidation in skeletal muscle and decreases lipogenesis in WAT, ultimately reducing ectopic fat deposition and adiposity (18). Consequently, AMPK acts as a central gauge in lipid and glucose homeostasis (1,2) and represents an attractive target for the treatment of obesity and T2DM (1).

Interestingly, AMPK activation by phosphorylation is promoted and stabilized by increased intracellular AMP:ATP and Cr:PCr ratios, which reflect cellular energy deficiency (3,4). Our study demonstrates that (P)Cr deficiency leads to reduced intracellular ATP levels and increased phosphorylation of AMPK and its downstream target ACC. At a functional level, elevated basal AMPK activation is characterized by decreased AICAR responses (Fig. 5). Furthermore, Cr supplementation normalizes pAMPK or pACC levels in AGAT-deficient mice, establishing a direct link between the (P)Cr pool and AMPK activity. Therefore, our mouse model represents a novel approach to chronic and systemic AMPK activation (Fig. 8).

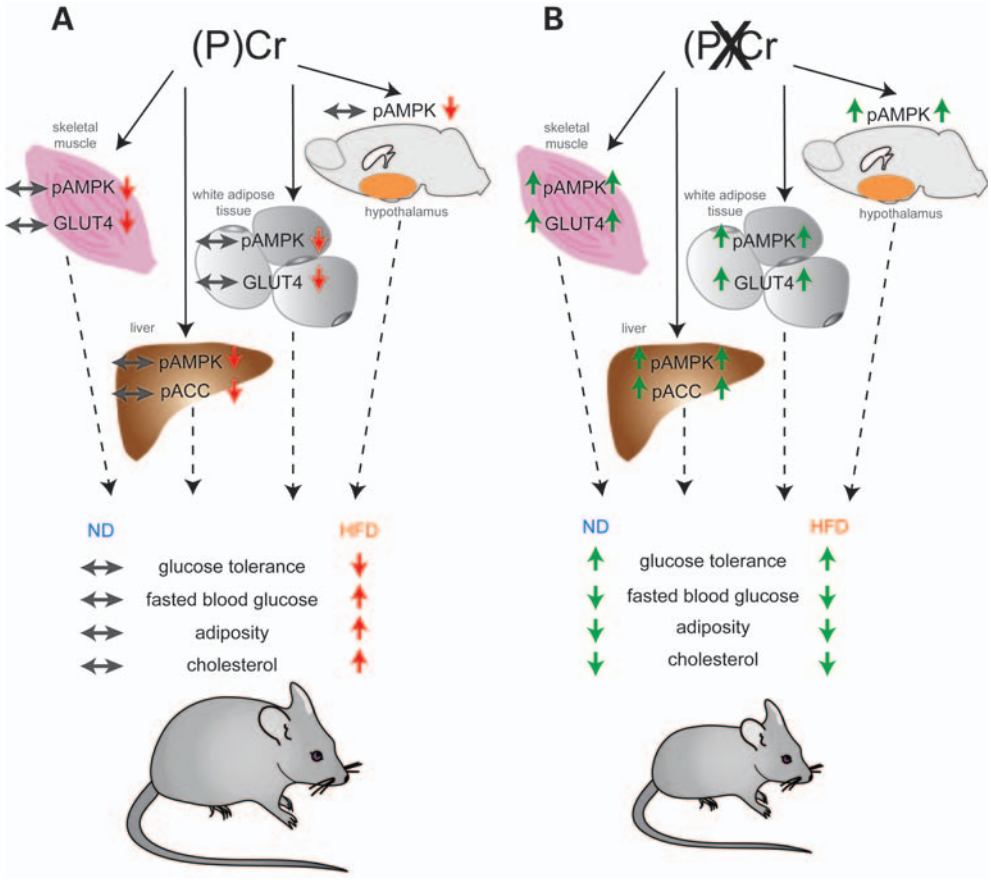

Figure 8. Schematic summary of AMPK activation and metabolic effects in normal and Cr-deficient mice. (**A**) Metabolic parameters change in wt mice on HFD. (**B**) Cr deficiency increases pAMPK and GLUT4 in skeletal muscle and WAT, as well as pAMPK levels in the liver and brain, regardless of the diet.

There are numerous transgenic mouse models of reduced or deficient AMPK activity, but only a limited number of chronic AMPK activation models that demonstrate marked effects of AMPK on lipid and glucose metabolism (19). Pharmacological approaches aimed at blocking ATP synthesis or mimicking AMP (e.g. AICAR) are known to exert unspecific effects on additional AMP-sensitive enzymes (glycogen phosphorylase, fructose-1,6-bisphosphatase) (14). Liver-specific expression of a constitutively active AMPK transgene resulted in reduced fat storage and reduced weight gain on high-fat diet (20–22), but rendered AMPK unresponsive to hormonal, nutrient and energy signals. Thus, AGAT d/d mice are the first genetic mouse model with chronic, systemic and reversible AMPK activation.

Cr-deficient mice are resistant to metabolic syndrome

Our data indicate that enhanced glucose tolerance and reduced lipid accumulation in Cr-deficient mice are presumably a consequence of chronic AMPK activation, leading to reduced adiposity, enhanced glucose tolerance and reduced cholesterol levels (Fig. 7). While other transgenic mouse models with increased AMPK activity revealed only moderate effects on DIO-associated weight change (still >50% weight gain) (22), AMPK activation in AGAT-deficient mice was associated with complete protection from DIO. Previous models of chronic AMPK activation expressed constitutively active AMPK subunits that were, for example, tissue specifically expressed in the liver (22), whereas our approach resulted in complete and systemic depletion of PCr and thus in AMPK activation. Mouse models of (P)Cr deficiency, i.e. GAMT$^{-/-}$ and CK-B/UbCKmit double-knockout mice, revealed decreased body weight and reduced adiposity (9,23). Inefficient neuronal transmission and defective thermoregulation have been suggested as underlying mechanisms in CK-B/UbCKmit double-knockout mice (23). Our current data suggest that reduced ATP levels in the absence of PCr and, consequently, chronic AMPK activation may account for the metabolic phenotype of mouse models with Cr deficiency. In addition to previous Cr deficiency models, our data indicate that Cr-dependent AMPK activation stimulates catabolic lipid metabolism with reduced lipid deposition and decreased cholesterol levels under conditions of HFD feeding.

Accumulating evidence suggests that the hypothalamus plays a pivotal and central role in the regulation of the whole-body energy metabolism. In particular, the AMPK signaling pathway in the hypothalamus is essential for energy homeostasis and glucose sensing (24). Previous studies demonstrated that hypothalamic AMPK inhibition suppressed glucose production, whereas hypothalamic AMPK stimulation increased hepatic gluconeogenesis (16,25). In contrast, we show that brain Cr deficiency results in chronic AMPK activation in

the hypothalamus and, as a consequence, in impaired glucose production. This discrepancy could be explained by the predominance of AMPK in specific neuronal subpopulations [e.g. those expressing proopiomelanocortin or neuropeptide Y and agouti-related protein (NPY/AgRP)] or tissues (e.g. hypothalamus versus liver) (26). The exact mechanism, however, remains elusive, because the relative contribution of neuronal subpopulations or tissues with chronic AMPK activation to the observed metabolic phenotype cannot be determined due to the systemic depletion of creatine in AGAT-deficient mice.

Unlike mouse models with liver-specific, constitutively active AMPK expression (22), our model shows that systemic Cr-dependent AMPK activation led to a reduction in body weight, cholesterol, blood glucose levels and a trend towards lower triglyceride levels. These marked effects on weight, adiposity and cholesterol levels were completely reversible on Cr supplementation, resulting in a normalization of AMPK activation parameters in the skeletal muscle, WAT and liver. Besides showing pronounced effects for lipid metabolism, our data suggest that (P)Cr depletion and subsequent AMPK activation in mice improve the glucose tolerance via different mechanisms and tissues. AMPK activation in the liver inhibits hepatic gluconeogenesis and thereby reduces the supply of glucose during fasting (27). In line with these results, our functional tests revealed a Cr-dependent inhibition of gluconeogenesis. In addition to reduced gluconeogenesis, plasmatic glucose clearance is also increased via elevated levels of GLUT4 in skeletal muscle and WAT. In our mouse model, improvement of glucose tolerance could not be attributed to either increased insulin secretion or increased insulin sensitivity. Interestingly, insulin levels were decreased in d/d mice after glucose injection, whereas glucagon levels were unchanged in d/d mice compared with wt and d/d + Cr. Despite a tight link between insulin-secreting β-cells and glucagon-secreting α-cells, our results indicate a distinct Cr-dependent regulation of pancreatic islet cells (13). Given its regulation by intracellular energy levels and AMPK, the K_{ATP} potassium channel seems a likely candidate linking the (P)Cr pool and islet cell function to sense glucose levels and secrete hormones (13). Thus, Cr-dependent AMPK activation is independent of insulin and could therefore therapeutically bypass insulin resistance.

In summary, we demonstrate that the chronic depletion of the (P)Cr pool in AGAT-deficient mice leads to AMPK activation and thereby to a reduction in BMI, enhanced glucose tolerance and complete protection from DIO. We conclude that AMPK activation via intracellular energy depletion reveals a putative mechanism for the treatment of obesity and T2DM.

MATERIALS AND METHODS

Generation of AGAT-deficient mice

In brief, AGAT-deficient knockout ($AGAT^{-/-}$) mice were generated by homologous recombination in mouse embryonic stem (ES) cells. The targeting vector comprised AGAT exons 3–7 subcloned from a 129/SvJ BAC clone containing the AGAT locus. Exon 3 was disrupted by insertion of a loxP-flanked neomycin selection cassette. The linearized targeting vector was electroporated into R1 ES cells, which were subjected to selection by geneticin (G418, Invitrogen, Karlsruhe, Germany). Homologous recombination was verified by Southern blot analysis of digested genomic ES cell DNA as described previously (9). Two positive clones were expanded and microinjected into C57BL/6J mouse blastocysts, which were then transferred into pseudo-pregnant CBA/C57BL/6J females. Two of the chimeric mice that were mated gave rise to germline transmission of the disrupted allele. To excise the neomycin selection cassette from the targeted allele, $AGAT^{+/-}$ were crossed with a cre deleter mouse line expressing cre recombinase in the germline. Males and females with different genotypes from different litters were randomly intercrossed to obtain $AGAT^{+/+}$, $AGAT^{+/-}$ and $AGAT^{-/-}$ progeny. Genomic DNA from mouse tail or ear biopsies was screened by either Southern analysis or multiplex polymerase chain reaction following the standard protocols.

Care and use of transgenic mice

Mice used in this study were obtained from heterozygous breeding after backcrossing to a C57BL/6J genetic background for at least six generations. All analyzed animals were littermates. Mice (<5 per cage) were kept in standard cages under a 12 h:12 h light:dark cycle, constant temperature and humidity and received standard food and water *ad libitum*. Chow was essentially Cr free (R/M-H, Ssniff) (9). Cr supplementation was achieved by addition of 1% Cr to chow (Ssniff) or drinking water. HFD contained 60 kJ% fat (Ssniff). All experimental procedures were approved by the respective local animal ethics committees (Hamburg: 110/10, Nijmegen: 2007-173).

In vivo ^{1}H and ^{31}P magnetic resonance spectroscopy

The metabolic profile of hind leg muscle was assessed *in vivo* by ^{1}H and ^{31}P magnetic resonance spectroscopy (MRS) on a horizontal bore magnet (Magnex Scientific) interfaced to a 7T MR spectrometer (MR Solutions), as described previously (28). Animals were anesthetized using 1.2% isoflurane (1/1 O_2/N_2O) and analyzed by *in vivo* ^{1}H and ^{31}P MRS. Localized ^{1}H MR spectra of the skeletal muscle of the lower hind limb positioned under the magic angle were acquired using a STEAM sequence (TR = 5 s, TE = 10 ms, TM = 15 ms, 128 averages, voxel size $1.8 \times 1.8 \times 3.8\ mm^3$) with VAPOR water suppression (29). Voxel position was determined on multislice gradient-echo images (TR = 250 ms, TE = 5 ms, field of view (FOV) $20 \times 20\ mm^2$, 256×256 matrix), and spectra were analyzed in the time domain using the jMRUI (http://www.mrui.uab.es) software package and water as an internal reference. One-dimensional-localized ^{31}P spectra of the hind leg were obtained using a three-turn solenoid coil and a pulse-acquire experiment (ISIS localization, 5 mm slice, TR = 7 s, 256 averages). NTP signal intensity was expressed as intensity per muscle volume as determined from the cross-sectional MR images in the corresponding slices.

Determination of guanidino compounds

Guanidino compounds were determined as described previously (9,30). Briefly, the guanidino compound concentrations

were determined with a Biotronic LC 5001 (Biotronik, Maintal, Germany) amino acid analyzer. All guanidino compounds were separated via a cation exchange column using sodium citrate buffers and were detected using the fluorescence ninhydrin method.

HTG and *de novo* lipogenesis

HTG content and its fractional synthesis by DNL were determined by $^{1}H/^{2}H$ NMR spectroscopy of liver extracts using $^{2}H_2O$ as a tracer aiming for 3% enrichment of body water over 18 h (31). Mice received an intraperitoneal injection with 99.9% $^{2}H_2O$ (Sigma-Aldrich, St Louis, MO, USA) followed by 18 h *ad libitum* access to ND chow and drinking water containing 3% $^{2}H_2O$. Lipids from freeze-clamped livers were separated by a Folch extraction followed by dissolution in chloroform (32). A detailed description of this method was reported previously (33). ^{1}H and ^{2}H NMR spectra were acquired on a 11.7 T NMR system (Bruker Instruments, Billerica, MA, USA) with WALTZ-16 decoupling. Enrichment of $^{2}H_2O$ and HTG was determined with TR = 10 s, 32 ave and TR = 4s and 2 K ave. MestreNova (MestreLab Research, Spain) was used for data processing. Total HTG and DNL fractions were quantified against the 1.1%-enriched $^{2}H_4$ pyrazine mixture as internal reference. The enrichment of HTG methyl hydrogens from $^{2}H_2$-enriched body water was used to calculate the contribution of DNL to the total HTG pool (33):

$$\text{Fraction DNL (in \%)} = \frac{[^{2}\text{H HTG}]}{^{2}\text{H body water}} \times 100$$

Glucose, AICAR, insulin and PTTs

Mice were fasted for 14–16 h and intraperitoneally injected with glucose (2 g/kg body weight), AICAR (0.25 g/kg body weight), insulin (0.5 U/kg body weight) or sodium pyruvate (2 g/kg body weight; Sigma-Aldrich). Blood glucose was measured from tail capillary blood and collected at indicated times. Blood glucose levels were determined using a glucometer (Accu-chek Sensor; Roche Diagnostics, Germany).

Urine analysis

For urine collection, mice were held over a clean Petri dish to elicit reflex urination. Urine produced was applied to a urine analysis reagent strips (Multistix® 10 SG Reagent Strips, Siemens, Germany) and scored on a color scale for glucose (negative, 100, 250, 500, 1000 and 2000 mg/dl).

Cage activity

Home cage activity was monitored for three consecutive days with an infrared motion detector (INFRA-E-MOTION). Activity levels were calculated as the sum of activity values obtained during light and dark phases.

Tissue collection and preparation

Animals were anesthetized with 2–3% isoflurane in 100% oxygen. Muscle and fat were removed and flash frozen in liquid nitrogen. Lysates were prepared in homogenization buffer containing phosphatase inhibitors with disposable 1.5-ml pestles (VWR) and cleared by centrifugation (34). Protein concentrations were determined using a BCA™ protein assay (Thermo Scientific).

Blood chemistry

Venous ethylenediaminetetraacetic acid blood was retrieved by submandibular puncture and heparinized blood by direct cardiac puncture. Plasma triglycerides and cholesterol levels were determined by standard laboratory methods based on certified assays employed in the Department of Clinical Chemistry, University Medical Center Hamburg-Eppendorf, using enzyme-based kits (Vitros Chemistry).

Determination of metabolic hormones

Leptin, insulin, fT3, adiponectin and glucagon plasma levels were measured by enzyme-linked immunosorbent assay according to the manufacturers' protocols (leptin, insulin: Crystal Chemistry; fT3: Calbiotech; adiponectin: BioCat; glucagon: Cusabio Biotech).

Western blots

Equal amounts of cleared lysates (20–40 μg protein) were separated by sodium dodecyl sulfatepolyacrylamide gel electrophoresis on precast gels (Invitrogen) and transferred to nitrocellulose membrane. Polyclonal rabbit antibodies against recombinant murine AGAT protein purified from *Escherichia coli* were kindly provided by Brian Tseng (Harvard University, USA). Antibodies against AMPKα, phospho-ACC (Ser79), phospho-AMPKα (Thr172) (Cell Signaling) and mouse anti-GLUT4 (Acris Antibodies) were used according to the manufacturers' protocols. Enhanced chemiluminescence (Luminata Crescendo, Millipore) signals were detected with a luminescent image analyzer (LAS-4000, FujiFilm). Total protein was measured with a laser scanner (FLA-9000 with LPG filter, FujiFilm) on blot membranes stained with Lava Purple (Fluorotechnics, GelCompany) according to the manufacturer's instructions (35). Signal quantification was performed on non-saturated images using ImageJ software (36).

Analysis of body composition

Body water was calculated as the difference before and after drying, lean mass was measured after chloroform extraction, the fat mass being the difference between dry and lean mass.

Liver morphology

To analyze liver tissue, mice were transcardially perfused with 4% paraformaldehyde in phosphate-buffered saline (PBS). Livers were carefully dissected and post-fixed in the same

solution at 4°C for 24 h. The tissue was cryoprotected in 30% sucrose in PBS and frozen in Jung tissue-freezing medium (Leica Microsystems) on dry ice. Liver sections were cut at 14 μm on a cryostat (Leica Microsystems). Lipids were stained with Sudan black.

Statistical analyses

Data are given as mean ± SEM. The following statistical tests were applied: parametric *t*-test (Excel X, Microsoft), one-way ANOVA, two-way ANOVA or ANOVA for repeated measurements, followed by Newman–Keuls *post hoc* comparisons (Statistica 5, Statsoft). All tests were two-tailed and the level of significance was set at $P < 0.05$.

SUPPLEMENTARY MATERIAL

Supplementary Material is available at *HMG* online.

ACKNOWLEDGMENTS

We wish to thank H. Voss, I. Heinsohn, S. Noster, N. Jäger and U. Wolters for expert animal care; M. Schweizer, C. Raithore and S. Fehr for help with histology/histochemistry; R. Peco Navio for help with the generation of AGAT knockout mice and preliminary phenotyping experiments, T. Streichert for help with blood chemistry (University Medical Center Hamburg-Eppendorf); J. Rozman for calorimetric and temperature measurements (German Mouse Clinic, Munich); B. Tseng (Harvard University, Boston, MA, USA) for providing the AGAT antiserum; B. Wieringa for helpful discussion (Radboud University, Nijmegen Medical Center).

Conflict of Interest statement. None declared.

FUNDING

This work was supported by the Deutsche Forschungsgemeinschaft (DFG) (CH872/1-1 to C.C., A.N. and D.I., IS63/3-1 and IS63/3-2 to D.I.) and by the Netherlands Organization for Scientific Research (NWO investment grant 834.04.008 to A.H.).

REFERENCES

1. Wyss, M. and Kaddurah-Daouk, R. (2000) Creatine and creatinine metabolism. *Physiol. Rev.*, **80**, 1107–1213.
2. Stöckler, S., Isbrandt, D., Hanefeld, F., Schmidt, B. and von Figura, K. (1996) Guanidinoacetate methyltransferase deficiency: the first inborn error of creatine metabolism in man. *Am. J. Hum. Genet.*, **58**, 914–922.
3. Item, C.B., Stockler-Ipsiroglu, S., Stromberger, C., Muhl, A., Alessandri, M.G., Bianchi, M.C., Tosetti, M., Fornai, F. and Cioni, G. (2001) Arginine:glycine amidinotransferase deficiency: the third inborn error of creatine metabolism in humans. *Am. J. Hum. Genet.*, **69**, 1127–1133.
4. Salomons, G.S., van Dooren, S.J., Verhoeven, N.M., Cecil, K.M., Ball, W.S., Degrauw, T.J. and Jakobs, C. (2001) X-linked creatine-transporter gene (SLC6A8) defect: a new creatine-deficiency syndrome. *Am. J. Hum. Genet.*, **68**, 1497–1500.
5. van Deursen, J., Heerschap, A., Oerlemans, F., Ruitenbeek, W., Jap, P., ter Laak, H. and Wieringa, B. (1993) Skeletal muscles of mice deficient in muscle creatine kinase lack burst activity. *Cell*, **74**, 621–631.
6. in 't Zandt, H.J., Renema, W.K., Streijger, F., Jost, C., Klomp, D.W., Oerlemans, F., Van der Zee, C.E., Wieringa, B. and Heerschap, A. (2004) Cerebral creatine kinase deficiency influences metabolite levels and morphology in the mouse brain: a quantitative in vivo 1H and 31P magnetic resonance study. *J. Neurochem.*, **90**, 1321–1330.
7. Jost, C.R., Van Der Zee, C.E., In 't Zandt, H.J., Oerlemans, F., Verheij, M., Streijger, F., Fransen, J., Heerschap, A., Cools, A.R. and Wieringa, B. (2002) Creatine kinase B-driven energy transfer in the brain is important for habituation and spatial learning behaviour, mossy fibre field size and determination of seizure susceptibility. *Eur. J. Neurosci.*, **15**, 1692–1706.
8. Steeghs, K., Benders, A., Oerlemans, F., de Haan, A., Heerschap, A., Ruitenbeek, W., Jost, C., van Deursen, J., Perryman, B., Pette, D. *et al.* (1997) Altered Ca2+ responses in muscles with combined mitochondrial and cytosolic creatine kinase deficiencies. *Cell*, **89**, 93–103.
9. Schmidt, A., Marescau, B., Boehm, E.A., Renema, W.K., Peco, R., Das, A., Steinfeld, R., Chan, S., Wallis, J., Davidoff, M. *et al.* (2004) Severely altered guanidino compound levels, disturbed body weight homeostasis and impaired fertility in a mouse model of guanidinoacetate N-methyltransferase (GAMT) deficiency. *Hum. Mol .Genet.*, **13**, 905–921.
10. Kan, H.E., Renema, W.K., Isbrandt, D. and Heerschap, A. (2004) Phosphorylated guanidinoacetate partly compensates for the lack of phosphocreatine in skeletal muscle of mice lacking guanidinoacetate methyltransferase. *J. Physiol.*, **560**, 219–229.
11. Ponticos, M., Lu, Q.L., Morgan, J.E., Hardie, D.G., Partridge, T.A. and Carling, D. (1998) Dual regulation of the AMP-activated protein kinase provides a novel mechanism for the control of creatine kinase in skeletal muscle. *EMBO J.*, **17**, 1688–1699.
12. Steinberg, G.R. and Kemp, B.E. (2009) AMPK in health and disease. *Physiol. Rev.*, **89**, 1025–1078.
13. Rorsman, P., Salehi, S.A., Abdulkader, F., Braun, M. and MacDonald, P.E. (2008) K(ATP)-channels and glucose-regulated glucagon secretion. *Trends Endocrinol. Metab.*, **19**, 277–284.
14. Towler, M.C. and Hardie, D.G. (2007) AMP-activated protein kinase in metabolic control and insulin signaling. *Circ. Res.*, **100**, 328–341.
15. Winder, W.W., Wilson, H.A., Hardie, D.G., Rasmussen, B.B., Hutber, C.A., Call, G.B., Clayton, R.D., Conley, L.M., Yoon, S. and Zhou, B. (1997) Phosphorylation of rat muscle acetyl-CoA carboxylase by AMP-activated protein kinase and protein kinase A. *J. Appl. Physiol.*, **82**, 219–225.
16. Kinote, A., Faria, J.A., Roman, E.A., Solon, C., Razolli, D.S., Ignacio-Souza, L.M., Sollon, C.S., Nascimento, L.F., de Araujo, T.M., Barbosa, A.P. *et al.* (2012) Fructose-induced hypothalamic AMPK activation stimulates hepatic PEPCK and gluconeogenesis due to increased corticosterone levels. *Endocrinology*, **153**, 3633–3645.
17. Neu, A., Neuhoff, H., Trube, G., Fehr, S., Ullrich, K., Roeper, J. and Isbrandt, D. (2002) Activation of GABA(A) receptors by guanidinoacetate: a novel pathophysiological mechanism. *Neurobiol. Dis.*, **11**, 298–307.
18. Long, Y.C. and Zierath, J.R. (2006) AMP-activated protein kinase signaling in metabolic regulation. *J. Clin. Invest.*, **116**, 1776–1783.
19. Ljubicic, V., Miura, P., Burt, M., Boudreault, L., Khogali, S., Lunde, J.A., Renaud, J.M. and Jasmin, B.J. (2011) Chronic AMPK activation evokes the slow, oxidative myogenic program and triggers beneficial adaptations in mdx mouse skeletal muscle. *Hum. Mol. Genet.*, **20**, 3478–3493.
20. Viana, A.Y., Sakoda, H., Anai, M., Fujishiro, M., Ono, H., Kushiyama, A., Fukushima, Y., Sato, Y., Oshida, Y., Uchijima, Y. *et al.* (2006) Role of hepatic AMPK activation in glucose metabolism and dexamethasone-induced regulation of AMPK expression. *Diabetes Res. Clin. Pract.*, **73**, 135–142.
21. Foretz, M., Ancellin, N., Andreelli, F., Saintillan, Y., Grondin, P., Kahn, A., Thorens, B., Vaulont, S. and Viollet, B. (2005) Short-term overexpression of a constitutively active form of AMP-activated protein kinase in the liver leads to mild hypoglycemia and fatty liver. *Diabetes*, **54**, 1331–1339.
22. Yang, J., Maika, S., Craddock, L., King, J.A. and Liu, Z.M. (2008) Chronic activation of AMP-activated protein kinase-alpha1 in liver leads to decreased adiposity in mice. *Biochem. Biophys. Res. Commun.*, **370**, 248–253.
23. Streijger, F., Pluk, H., Oerlemans, F., Beckers, G., Bianco, A.C., Ribeiro, M.O., Wieringa, B. and Van der Zee, C.E. (2009) Mice lacking brain-type creatine kinase activity show defective thermoregulation. *Physiol. Behav.*, **97**, 76–86.

24. Claret, M., Smith, M.A., Batterham, R.L., Selman, C., Choudhury, A.I., Fryer, L.G., Clements, M., Al-Qassab, H., Heffron, H., Xu, A.W. *et al.* (2007) AMPK is essential for energy homeostasis regulation and glucose sensing by POMC and AgRP neurons. *J. Clin. Invest.*, **117**, 2325–2336.
25. Yang, C.S., Lam, C.K., Chari, M., Cheung, G.W., Kokorovic, A., Gao, S., Leclerc, I., Rutter, G.A. and Lam, T.K. (2010) Hypothalamic AMP-activated protein kinase regulates glucose production. *Diabetes*, **59**, 2435–2443.
26. Belgardt, B.F., Okamura, T. and Bruning, J.C. (2009) Hormone and glucose signalling in POMC and AgRP neurons. *J. Physiol.*, **587**, 5305–5314.
27. Lochhead, P.A., Salt, I.P., Walker, K.S., Hardie, D.G. and Sutherland, C. (2000) 5-aminoimidazole-4-carboxamide riboside mimics the effects of insulin on the expression of the 2 key gluconeogenic genes PEPCK and glucose-6-phosphatase. *Diabetes*, **49**, 896–903.
28. Renema, W.K., Schmidt, A., van Asten, J.J., Oerlemans, F., Ullrich, K., Wieringa, B., Isbrandt, D. and Heerschap, A. (2003) MR spectroscopy of muscle and brain in guanidinoacetate methyltransferase (GAMT)-deficient mice: validation of an animal model to study creatine deficiency. *Magn. Reson. Med.*, **50**, 936–943.
29. in 't Zandt, H.J., Klomp, D.W., Oerlemans, F., Wieringa, B., Hilbers, C.W. and Heerschap, A. (2000) Proton MR spectroscopy of wild-type and creatine kinase deficient mouse skeletal muscle: dipole-dipole coupling effects and post-mortem changes. *Magn. Reson. Med.*, **43**, 517–524.
30. Marescau, B., Deshmukh, D.R., Kockx, M., Possemiers, I., Qureshi, I.A., Wiechert, P. and De Deyn, P.P. (1992) Guanidino compounds in serum, urine, liver, kidney, and brain of man and some ureotelic animals. *Metabolism*, **41**, 526–532.
31. Jones, J.G., Merritt, M. and Malloy, C. (2001) Quantifying tracer levels of (2)H(2)O enrichment from microliter amounts of plasma and urine by (2)H NMR. *Magn. Reson. Med.*, **45**, 156–158.
32. Folch, J., Lees, M. and Sloane Stanley, G.H. (1957) A simple method for the isolation and purification of total lipides from animal tissues. *J. Biol. Chem.*, **226**, 497–509.
33. Delgado, T.C., Pinheiro, D., Caldeira, M., Castro, M.M., Geraldes, C.F., Lopez-Larrubia, P., Cerdan, S. and Jones, J.G. (2009) Sources of hepatic triglyceride accumulation during high-fat feeding in the healthy rat. *NMR Biomed.*, **22**, 310–317.
34. Nakken, G.N., Jacobs, D.L., Thomson, D.M., Fillmore, N. and Winder, W.W. (2010) Effects of excess corticosterone on LKB1 and AMPK signaling in rat skeletal muscle. *J. Appl. Physiol.*, **108**, 298–305.
35. Mackintosh, J.A., Choi, H.Y., Bae, S.H., Veal, D.A., Bell, P.J., Ferrari, B.C., Van Dyk, D.D., Verrills, N.M., Paik, Y.K. and Karuso, P. (2003) A fluorescent natural product for ultra sensitive detection of proteins in one-dimensional and two-dimensional gel electrophoresis. *Proteomics*, **3**, 2273–2288.
36. Abramoff, M.D., Magelhaes, P.J. and Ram, S.J. (2004). Image Processing with Image J. *Biophotonics Int*, **11**, 36–42